ACS OMEGA

Open Access

http://pubs.acs.org/journal/acsodf

Article

Study on Control Strategies on NO_X Emissions to Meet Real Driving Emissions

Jing Chen, Yan Su,* Li Xiaoping, Fangxi Xie, Yongzhen Wang, and Chuang Yang

Cite This: *ACS Omega* 2023, 8, 47452−47462

Read Online

ACCESS | Metrics & More | Article Recommendations

ABSTRACT: The aim of this study was to fulfill the NOx emissions standards for a light-duty diesel vehicle under real driving emissions (RDE) testing conditions by implementing various control strategies. In this study, RDE tests were performed by adjusting the air mass quantity and postinjection quantity in order to analyze engine-out and tail-pipe nitrogen oxides (NOx) emissions for different phases of RDE. The results showed that reducing in air mass quantity enabled the engine to operate in higher exhaust gas recirculation (EGR) rate regions, resulting in a 32.5% reduction in engine-out NOx emissions and an 80.4% decrease in tail-pipe NOx emissions. Increasing the postinjection quantity primarily enhanced the NOx conversion efficiency for the urban phase by 7.5%, leading to a 22.6% reduction in tail-pipe NOx emissions. By employing both strategies, vehicles can comfortably meet the CN6b emission regulations by a substantial margin.

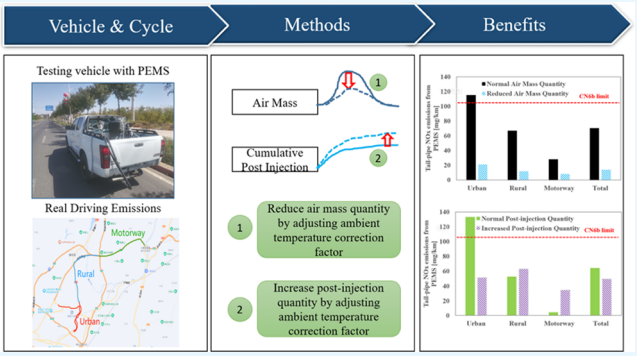

1. INTRODUCTION

Vehicular emissions, encompassing carbon monoxide (CO), carbon dioxide (CO_2), total hydrocarbons (THC), and nitrogen oxides (NOx), have been acknowledged as detrimental to both human well-being and the environment.[1,2] Automobiles emerged as the predominant source of pollution, constituting approximately 39% of the aggregate NOx emissions in 2016.[3] Furthermore, diesel vehicles are considered a major global contributor to NOx.[4] It is widely agreed that decreasing NOx emissions from diesel vehicles would have positive implications for both human well-being and environmental preservation. To fulfill the increasingly stringent emission regulations for the future, diesel vehicles require optimized methods that combine in-cylinder purification and efficient exhaust after-treatment technologies. Generally, the formation of NOx in the cylinder is related to the combustion efficiency. This can be achieved through various means including the utilization of a steel piston with an innovative bowl geometry,[5] implementing the Miller cycle with variable compression ratio function,[6] adopting new clean energy sources like methyl ester fuel[7] and hydrotreated vegetable oil,[8] introducing exhaust gas recirculation (EGR),[9] and the meticulous calibration of injection parameters such as pilot injection,[10] injection timing,[11] and duration and fuel amount.[12] To effectively tackle NOx emissions, after-treatment techniques such as selective catalytic reduction (SCR),[13] an SCR catalyst-coated diesel particulate filter (SDPF),[14] and a lean NOx trap (LNT)[15] are employed for the conversion of NOx emissions.

The worldwide harmonized light-duty test cycle (WLTC) was developed and implemented within the current regulations, which incorporates more complex and variable operating conditions to better reflect vehicle economy and emissions performance,[16] but the discrepancy between laboratory tests and real-world measurements presents significant challenges to the control of harmful NOx emissions from vehicles;[17] many countries, such as European countries, South Korea, China, and Japan, have adopted the real driving emissions (RDE) testing protocol using Portable Emissions Measurement Systems (PEMS) to minimize the gap between on-road and laboratory emissions.[18−21] The results of emissions from on-road driving conditions are affected by driving conditions,[22−24] after-treatment systems,[14] routes,[19] environmental conditions,[25] and control strategies. There are two main NOx control technologies used in the car market: in-cylinder optimization technologies in concert with EGR and after-treatment systems. Control strategies, such as employing solely EGR through a transient control of model-based engine charge control (MCCT),[26] recalibrating EGR, utilizing various combinations like LNT + DPF or two diesel oxidation catalysts

Received: May 28, 2023
Revised: October 21, 2023
Accepted: November 22, 2023
Published: December 8, 2023

(DOC) + SDPF,[27] as well as implementing advanced NOx storage and reduction (NSR) technologies,[21] have been embraced to comply with the more stringent RDE regulations. Nevertheless, there has been limited investigation into the analysis of emissions correlations based on the control characteristics of the engine control unit (ECU).

This study analyzed the results of NOx utilizing a PEMS under real driving emissions testing conditions for emissions testing. Furthermore, this study obtained ECU signals and simultaneously measured NOx emissions upstream and downstream of the catalyst in the test vehicle by using NOx sensors. In contrast to prior studies, this study specifically examined the impact of adjusting the ECU control strategies on the engine-out and tail-pipe NOx emissions to achieve compliance with real driving emissions standards.

2. EXPERIMENTAL PROCEDURE

2.1. Experimental Setup. The commercial vehicle used for the experiments is equipped with a diesel engine with a nominal volume displacement of 2.5 L and a rated power of 105 kW. The after-treatment system comprises a diesel oxidation catalyst (DOC), selective catalytic reduction (SCR), and an SCR catalyst-coated diesel particulate filter (SDPF). More details of the vehicle specifications and vehicle system layout are shown in Table 1 and Figure 1, respectively.

Table 1. Vehicle Specifications

specifications	test vehicle
vehicle model	Isuzu Ruimai
fuel type	diesel
curb weight (t)	2.04
engine type	turbocharged, direct injection
engine power (kW/Nm)	105/360
displacement (L)	2.5
after-treatment	DOC + SDPF + SCR
emission standard	CN6b
gear	manual 6
model year	2022
odometer (km)	3200

2.2. Experimental Program. The decrease in NOx emissions from vehicles can be done by both reducing engine-out NOx emissions and improving the after-treatment conversion efficiency. On the one hand, this study proposed reducing engine-out NOx emissions by varying the air mass quantity. On the other hand, this study reduced NOx emissions by adding the postinjection quantity to increase the engine exhaust temperature to improve the after-treatment conversion efficiency. In this study, the tests without and with the reduction in air mass quantity and without and with the increase in postinjection quantity were labeled as test 1, test 2, test 3, and test 4, respectively. In addition, test 1 and test 2 were tested using one reference CO_2 quantity, while test 3 and test 4 used another reference CO_2 quantity.

The overview of model-based engine charge control (MCC) used in this paper is shown in Figure 2. The air control (AirCtl) component sets the charge of the engine with fresh air and recirculated exhaust gas according to the demands of the current operating mode and the current operating point. The actuators controlled by the component are the EGR and throttle valves. The fresh air mass and the EGR rates are adjusted simultaneously with these two actuators. In this air system control model, the desired air mass quantity is the input and the EGR valve open rate is the output. The desired air mass quantity is calculated as follows

$$m_{des} = \eta_{ats1} \cdot m_{ats} + \eta_{aps1} \cdot m_{aps} + \eta_{ets1} \cdot m_{ets} + m_{bas} \quad (1)$$

where m_{des} is the desired air mass quantity in units of milligrams per stroke, mg/str; η_{ats1} is the factor corrected by ambient temperature; m_{ats} is the corrected air mass quantity by ambient temperature in units of milligrams per stroke, mg/str; η_{aps1} is the factor corrected by ambient pressure; m_{aps} is the corrected air mass quantity by ambient pressure in units of milligrams per stroke, mg/str; η_{ets1} is the factor corrected by engine temperature; m_{ets} is the corrected air mass quantity by engine temperature in units of milligrams per stroke, mg/str; and m_{bas} is the base air mass in units of milligrams per stroke, mg/str.

Considering the practical performance, this paper adjusts the ambient temperature correction factor (η_{ats1}) to reduce the air mass quantity. Figure 3 shows the ambient temperature correction factor map of tests 1 and 2. The main adjustment area is the area where the engine speed is between 750 and 2750 rpm and the ambient temperature is between −15 and 11 °C.

Postinjection is an injection situated after the main injection, used to burn off the soot in the combustion chamber and for the regeneration of exhaust gas treatment systems. The postinjection quantity is calculated by several correction factors and static postinjection quantity. These correction factors are used to modify the static postinjection quantity, which contains corrections for engine temperature, ambient temperature, and ambient pressure. The desired postinjection quantity is calculated as follows

$$q_{poi} = \eta_{ats2} \cdot q_{ats} + \eta_{aps2} \cdot q_{aps} + \eta_{ets2} \cdot q_{ets} + q_{bas} \quad (2)$$

where q_{poi} is the desired postinjection quantity in units of milligrams per stroke, mg/str; η_{ats2} is the factor corrected by ambient temperature; q_{ats} is the corrected postinjection quantity by ambient temperature in units of milligrams per stroke, mg/str; η_{aps2} is the factor corrected by ambient pressure; q_{aps} is the corrected postinjection quantity by ambient pressure in units of milligrams per stroke, mg/str; η_{ets2} is the factor corrected by engine temperature; q_{ets} is the corrected postinjection quantity by engine temperature in units of milligrams per stroke, mg/str; and q_{bas} is the base postinjection quantity in units of milligrams per stroke, mg/str.

Considering the practical performance, this paper corrected the postinjection quantity based on ambient temperature as shown in Figure 4. The main difference is that test 4 adds the postinjection quantity corrected by ambient temperature, and it only works in the regions of total fuel injection quantity of 20−40 mg/str and engine speed of 1300−1600 rpm.

2.3. CN6b Regulations. CN6b regulations for light-duty vehicles provide for on-road emissions testing via PEMS to supplement the dynamometer-based type approval process to minimize the difference between laboratory and real emissions.[28] Both urban and total trip pollutant emissions should be less than exceed limits (NTE), calculated as eq 3, and no modifications should be made in the calculation process.

$$NTE_{NO_x} = CF_{NO_x} \times CN6b_{NO_x} \quad (3)$$

https://doi.org/10.1021/acsomega.3c03751
ACS Omega 2023, 8, 47452−47462

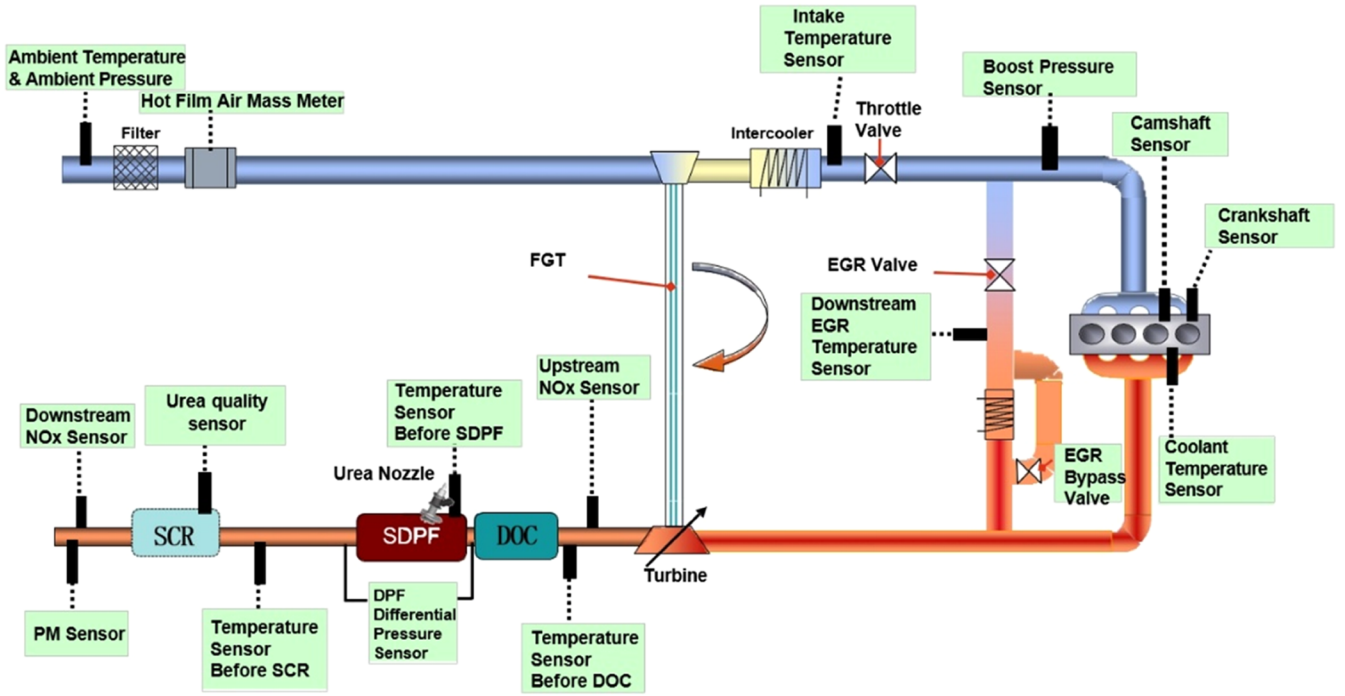

Figure 1. System layout of the test vehicle.

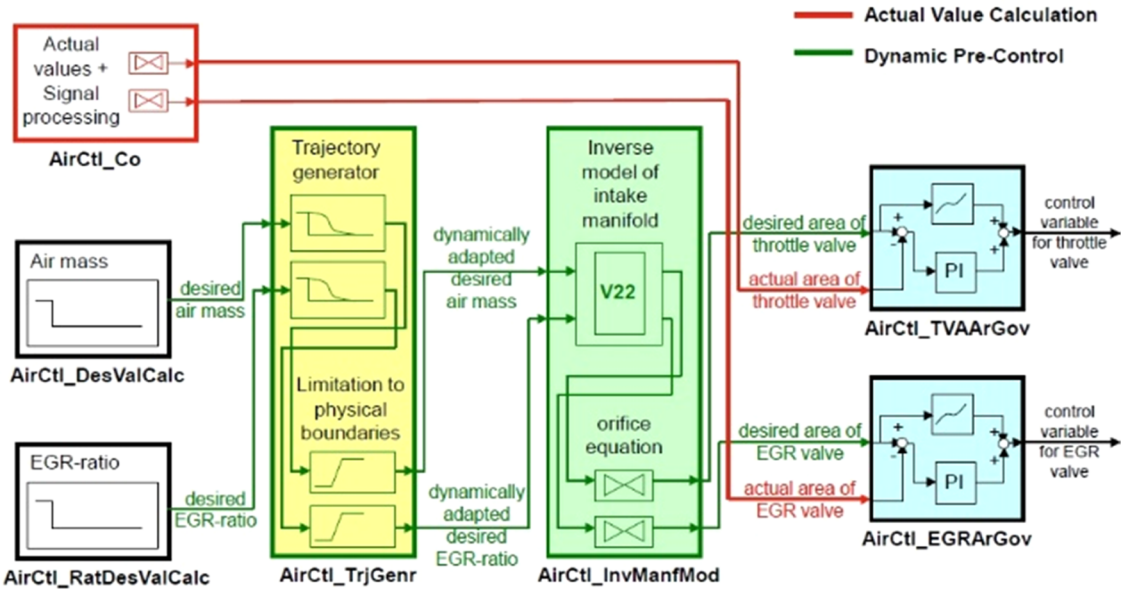

Figure 2. Overview of model-based engine charge control.

where CF_{NO_x} represents the conformity factor of NOx emissions, which is 2.1; $CN6b_{NO_x}$ represents the CN6b limit for NOx emissions, which is 50 mg/km.

For a trip to be qualified for RDE-type approval, the requirements of driving route, driving experiments, and test run must be fulfilled. As for the requirements of the driving route, an RDE trip must cover three phases based on vehicle speed: urban at speeds below 60 km/h, rural at speeds between 60 and 90 km/h, and motorway at speeds above 90 km/h. And the test should be performed consecutively in the order of urban, rural, and motorway. As for the requirements of the driving experiments, an RDE test should be performed on a paved surface or on the street. The PEMS shall be powered by an external power source and shall not be directly or indirectly from the engine of the test vehicle. The engine of the test vehicle was kept from idling for a long time after the first ignition and before the emission test begins. If the engine stalls unexpectedly during the test, then the engine should be restarted, with no interruption of the sampling of pollutants. The vehicle should avoid prolonged idling after the test trip. As for the requirements of the test run, sampling, measuring, and recording should be carried out continuously throughout the vehicle road test. The engine may be stopped and restarted during the test, but emissions sampling and recording should be performed continuously. The recorded data shall be 99% of the complete signal with no more than 1% of the total driving

https://doi.org/10.1021/acsomega.3c03751
ACS Omega 2023, 8, 47452−47462

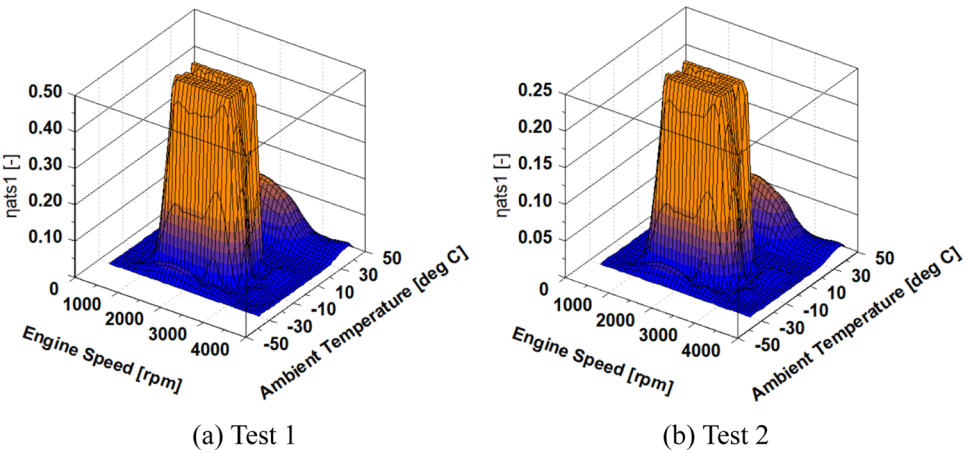

(a) Test 1 (b) Test 2

Figure 3. Ambient temperature correction factor map of air mass quantity control.

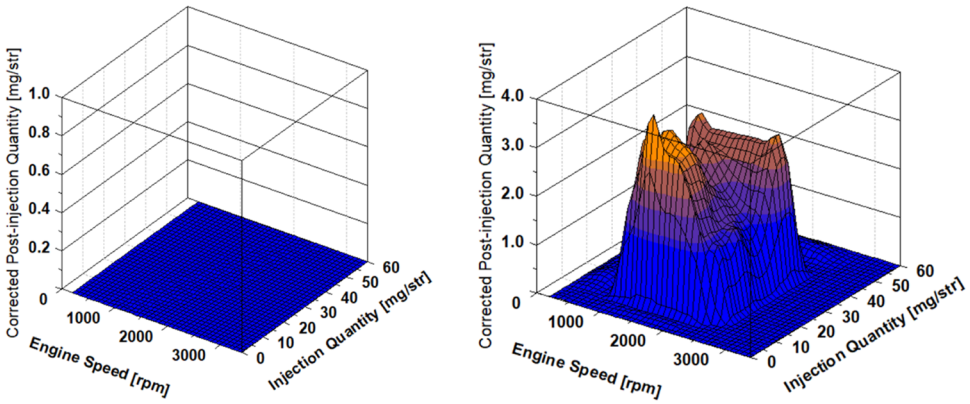

(a) Test 3 (b) Test 4

Figure 4. Postinjection quantity based on ambient temperature correction.

time interrupted by the data and no more than 30 s of continuous interruption; otherwise, the trip is judged invalid.

2.4. RDE Test Route. According to the RDE test protocol, the test should be performed consecutively in the order of urban, rural, and motorway, at least 16 km in each speed range, with the total time of the test between 90 and 120 min. The tests were conducted in Kunming, where the driving routes recorded by GPS are shown in Figure 5, including urban (the red route), rural (the blue route), and motorway (the green route). The test route was chosen to meet the RDE experimental requirements.

2.5. RDE Calculation and Trip Evaluation.

(1) The moving averaging window (MAW) method

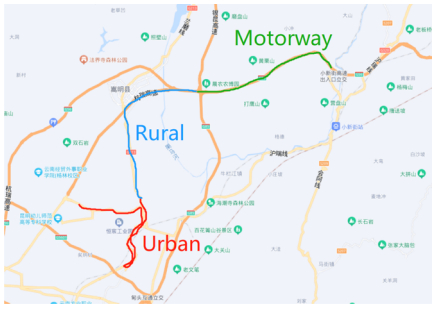

Figure 5. Topographic maps of the RDE test route.

By RDE test regulations, the calculation of emissions from light-duty vehicles requires time correction of pollutant concentrations, exhaust mass flow, vehicle speed, and other transient data recorded during the experiment. After that, cold start and engine off determinations were made, which were excluded from the subsequent data processing, as required by the MAW method.

The MAW method is a method for analyzing real driving pollutant emissions (RDE), which divides the experimental results into several subsets of data, or different windows, and uses statistical data processing to identify the effective RDE windows. The MAW method determines windows by the accumulated CO_2 emissions based on half of the total amount of CO_2 emissions from the WLTC.

In the calculation of the MAW method, it is necessary to evaluate the window normality with the CO_2 characteristic curve. The CO_2 emission results from each phase of the WLTC are weighted by coefficients of 1.2, 1.1, and 1.05, respectively, which are assigned to points P_1, P_2, and P_3, respectively. The parameters of P_1, P_2, and P_3 are determined by the average value of the vehicle speed and CO_2 emission coefficient of the vehicle in the low, high, and extra-high phases of the WLTC, and the three points are connected to form the CO_2 characteristic curve of the vehicle. If the CO_2 emission of a window lies above the curve, then it suggests that driving is more aggressive than normal driving. The basic and extended tolerances of the CO_2 characteristic curves are defined as tol1

https://doi.org/10.1021/acsomega.3c03751
ACS Omega 2023, 8, 47452−47462

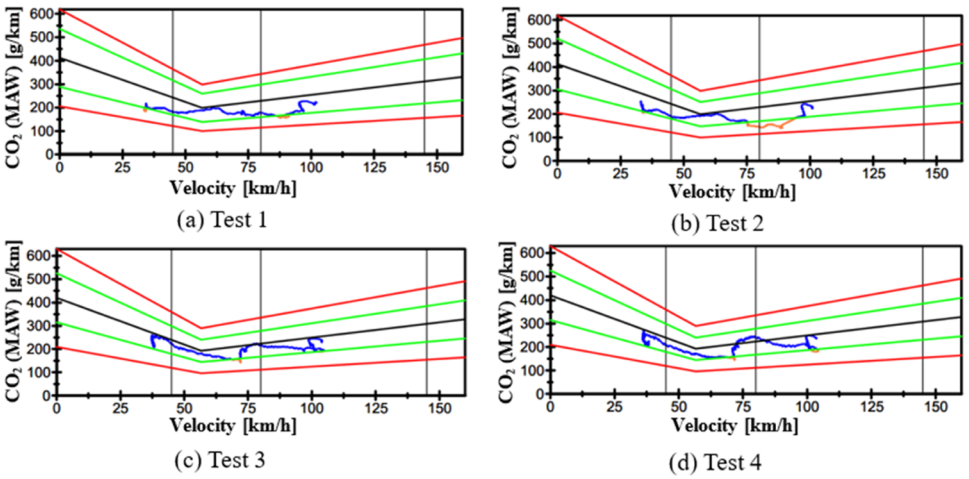

Figure 6. CO_2 characteristic curves of the RDE tests.

equal to 25% and tol2 equal to 50%, respectively. The CO_2 characteristic curves of all tests are shown in Figure 6.

The RDE experimental protocol requires that the results are judged to be normal when more than 50% of the urban, rural, and motorway windows fall within the basic tolerance range defined by the characteristic curve. If not, the upper limit of tol1 can be increased in 1% steps until the 50% window requirement is met. However, when using this method, tol1 must not eventually exceed 50%. The window normality verification is shown in Table 2.

Table 2. CO_2 Window Normality

test number	urban/%	rural/%	motorway/%	tol1/%
test 1	70.3	100	79.9	30
test 2	77.4	69.4	50.4	26
test 3	100	79.3	99.4	25
test 4	100	86.7	93.4	25

(2) Dynamics parameter verification

RDE regulations require that the acceleration degree, a_{pos} (positive acceleration greater than 0.1 m/s^2), and RPA be calculated based on the vehicle speed greater than 3 km/h, with an accuracy of 0.1% and a sampling frequency of 1 Hz or more. This study's PEMS acquisition signal meets the above accuracy and sampling frequency requirements. The time step of 1 s was chosen for the calculation of the dynamics parameters. Besides, the number of data sets with acceleration values above 0.1 m/s^2 in each velocity group should not be less than 150. The number of data sets with acceleration values above 0.1 m/s^2 of tests is shown in Figure 7. From Figure 7, the number of road sections in all RDE tests meets the requirements, in which the number of data sets with acceleration values above 0.1 m/s^2 in urban is over 1000, for rural, 400 to 600, and for motorway, 300 to 400.

In the CN6b regulation, the 95th percentile of the product of vehicle speed and positive acceleration greater than 0.1 m/s^2 and RPA is used to verify the trip dynamic conditions, with the former being used to eliminate the effects of excessively aggressive driving and the latter being used to eliminate the influence of excessively soft driving.

The RPA can be calculated as in eq 4,

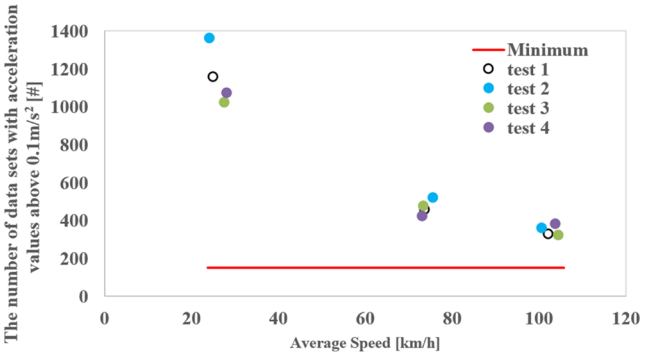

Figure 7. Number of data sets with acceleration values above 0.1 m/s^2 in each velocity group in RDE tests.

$$\mathrm{RPA}_k = \sum_j \Delta t \cdot (v \cdot a_{\mathrm{pos}})_{j,k} / \sum_i \mathrm{d}_{i,k} j = 1 \sim M_k \quad , i = 1 \sim N_k,\ k = u, r, m \tag{4}$$

where RPA_k is the RPA for the urban, rural, and motorway phases; Δt is the time step equal to 1 s; $\mathrm{d}_{i,k}$ is the distance covered in time step i for phase k; M_k is the sample number with positive acceleration in each phase; and N_k is the total sample number in each phase.

The RDE experiment requires verification of the 95th percentile of the product of vehicle speed and positive acceleration and RPA in each velocity group, defined as in eqs 5−8, where $\overline{v_k}$ is the average velocity in each phase. The trip decision is invalid if any of the following equations are satisfied

for

$$\overline{v_k} \le 74.6 \text{ km/h},\ (v \cdot a_{\mathrm{pos}})_k\_[95] > (0.136 \cdot \overline{v_k} + 14.44) \tag{5}$$

for

$$\overline{v_k} > 74.6 \text{ km/h},\ (v \cdot a_{\mathrm{pos}})_k\_[95] > (0.0742 \cdot \overline{v_k} + 18.966) \tag{6}$$

for $\overline{v_k} \le 94.05$ km/h, $\mathrm{RPA}_k < (-0.0016 \cdot \overline{v_k} + -0.1755)$ (7)

for $\overline{v_k} > 94.05$ km/h, $\mathrm{RPA}_k < 0.025$ (8)

https://doi.org/10.1021/acsomega.3c03751
ACS Omega 2023, 8, 47452−47462

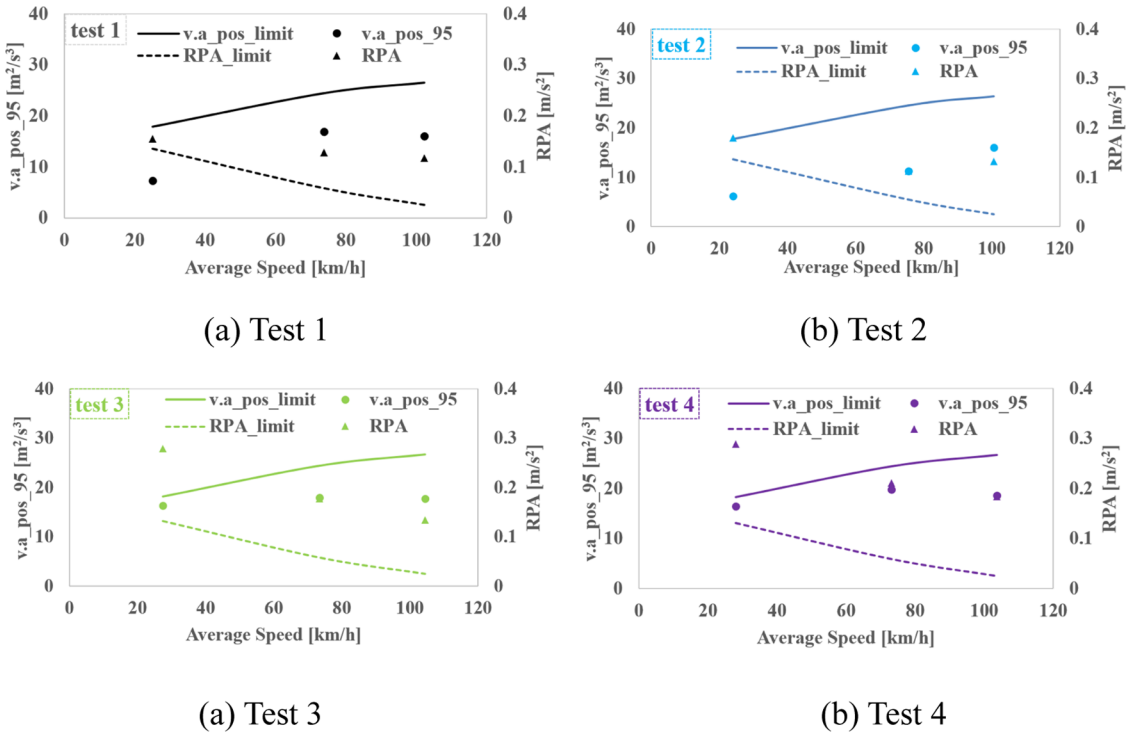

Figure 8. Dynamic boundaries of tests.

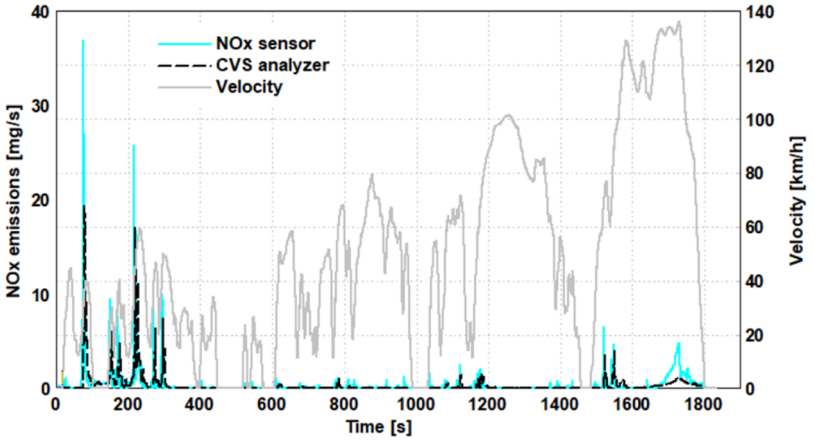

Figure 9. Comparison of NOx emissions measured by a NOx sensor and CVS analyzer.

The 95th percentile of the product of vehicle speed and positive acceleration and RPA of 4 experiments are shown in Figure 8. It can be seen from Figure 8 that the values from the tests do not exceed the limit of the RPA boundary and cross the limit of the 95th percentile of the product of vehicle speed and positive acceleration. The dynamic conditions showed that tests 1 and 2 were conducted under soft driving conditions, while tests 3 and 4 were conducted under aggressive driving conditions. In addition, as shown in Figures 6 and 8, both test 1 and test 2 are under soft driving conditions and show similar CO_2 characteristic curves under soft driving conditions, suggesting that both tests were conducted under similar driving conditions. Similarly, it can be concluded that tests 3 and 4 were also conducted under similar driving conditions.

3. RESULTS AND DISCUSSION

3.1. Difference between NOx Sensor Values and PEMS Values. As shown in Figure 1, the vehicle tested has a

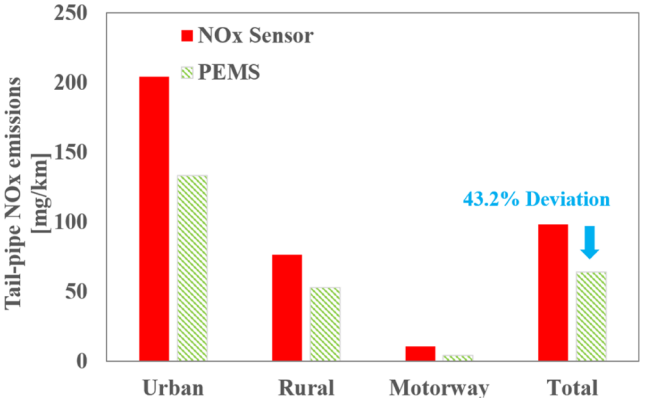

Figure 10. Difference between NOx sensor values and PEMS values in an RDE result.

https://doi.org/10.1021/acsomega.3c03751
ACS Omega 2023, 8, 47452−47462

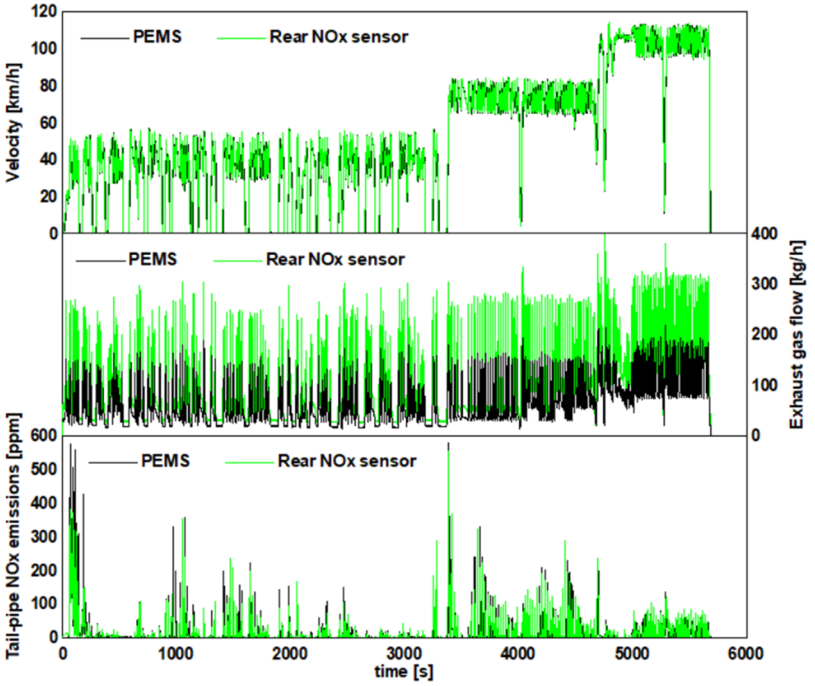

Figure 11. Vehicle speed, exhaust gas flow, and tail-pipe NOx emissions in terms of time from ECU and PEMS.

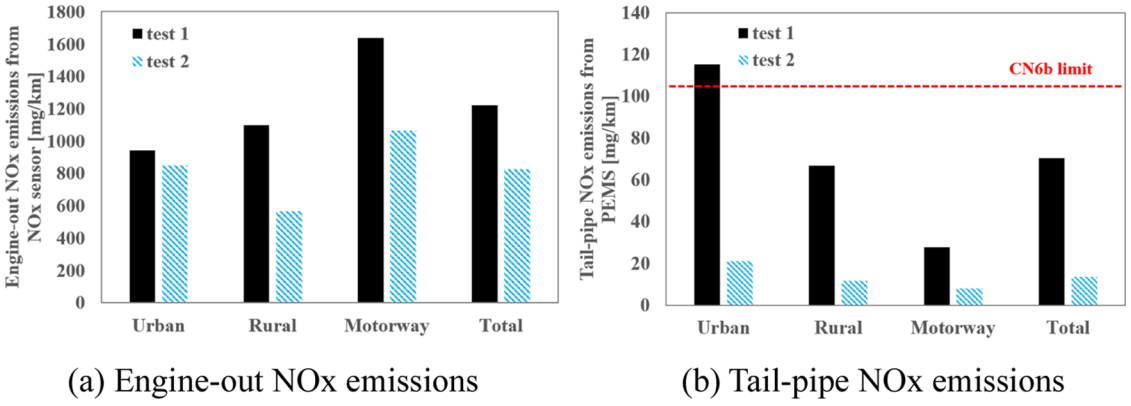

Figure 12. Comparison of engine-out and tail-pipe NOx emissions between test 1 and test 2.

NOx sensor installed in the front of the DOC to measure the vehicle's engine-out NOx emissions and has a NOx sensor installed in the rear of the SCR to measure the NOx emissions after the exhaust gas has been converted. Figure 9 shows the results of the test vehicle in the worldwide harmonized light-duty test cycle (WLTC). It can be seen from Figure 9 that the dynamic responsiveness of the NOx sensor values is consistent with the CVS analyzer values with very small differences in values.

In addition, the unit of the values of the NOx sensor is parts per million (ppm), so the following equation is introduced to convert parts per million to grams per kilometer (mg/km)

$$\dot{m}_{NOx} = C_{NOx} \cdot \dot{m}_{exh} \cdot \left(\frac{M_{NOx}}{M_{exh}}\right) \cdot \frac{10^6}{3600} \quad (9)$$

where $\dot{m}_{NOx}$ is the mass flow of NOx in units of milligrams per second, mg/s; C_{NOx} is the concentration of NOx in units of ppm measured by the NOx sensor, ppm; $\dot{m}_{exh}$ is the mass flow of exhaust in units of kilograms per hour read by integrated calibration and application tools (INCA), kg/h; M_{NOx} is the molecular weight of NOx with the value of 46; and M_{exh} is the molecular weight of exhaust gas with the value of 29.

$$m_{NOx} = \frac{\int_0^{1800} \dot{m}_{NOx} dt}{L} \quad (10)$$

where m_{NOx} is the NOx emissions in units of milligrams per kilometer, mg/km; and L is the vehicle's total mileage under the cycle in units of kilometers, km.

Taking the results of an RDE test as an example, Figure 10 shows that the calculated values of the NOx sensor differ greatly from the value of the PEMS. The total tail-pipe NOx emissions calculated by the NOx sensor in mg/km showed a deviation of 43.2% compared to the PEMS values because the NOx value in milligrams per km is related to the NOx value in ppm and the exhaust gas flow, which can be seen in eq 9. Figure 11 shows the vehicle speed, exhaust gas flow, and tail-pipe NOx emissions in terms of time from ECU and PEMS. As can be seen in Figure 11, the rear NOx sensor exhibits very little variability in the tail-pipe NOx emissions in ppm compared to PEMS, but the exhaust gas flow is much higher,

https://doi.org/10.1021/acsomega.3c03751
ACS Omega 2023, 8, 47452−47462

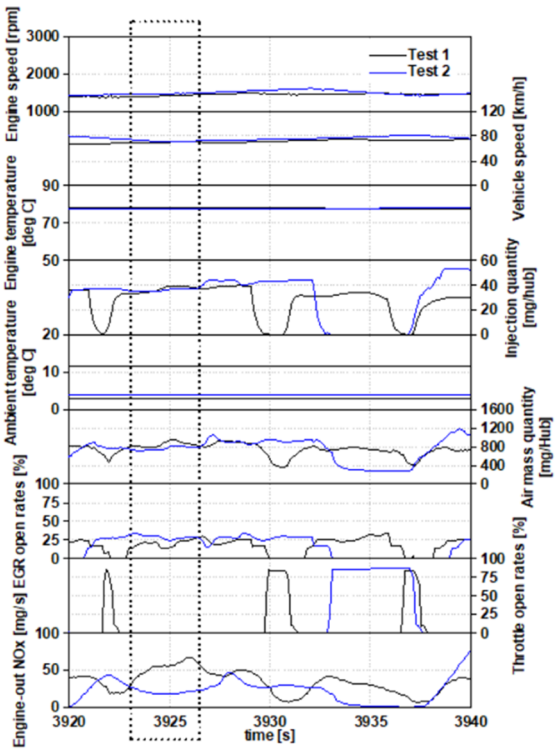

(a) Rural condition

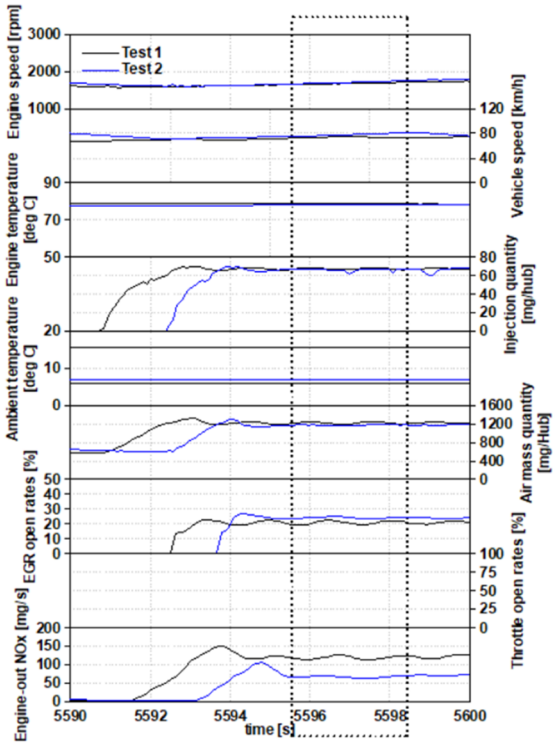

(b) Motorway condition

Figure 13. Comparison of rural and motorway conditions between test 1 and test 2; the black curve represents test 1 and the blue curve represents test 2.

resulting in a much larger calculated tail-pipe NOx emission in mg/km. Because of this variability, this paper uses NOx sensor values in ppm or mg/km for analysis and PEMS values as the evaluation criteria for regulation adoption.

3.3. Effect of Air Mass Quantity on NOx Emissions. This section presents the analysis of air mass quantity on engine-out and tail-pipe NOx emissions. The analysis was based on simultaneous NOx emissions measured upstream of the catalyst and values measured by the PEMS. Figure 12 results demonstrate a significant reduction in engine-out and tail-pipe NOx emissions for the RDE tests. Calculated from the front NOx sensor measurements, test 1 emits engine-out NOx emissions in total 1.48 times higher than those of test 2. This is mainly because compared to test 1, test 2 emits less engine-out NOx emissions for all of the phases of the RDE test, with 1.1, 1.95, and 1.54 times lower for urban, rural, and highway, respectively. As for the tail-pipe NOx emissions measured by the PEMS, the total NOx emissions of test 2 are 5.11 times lower than those of test 1, with 5.44, 5.62, and 3.46 times lower for urban, rural, and highway, respectively. In addition, test 2 with a reduced air mass quantity can meet the CN6b emission regulations by a significant margin, while test 1 fails because of the poor performance in the urban phase. This is because in the air system control model, the desired air mass quantity is the input and the EGR valve open rate is the output. The decrease in air mass quantity causes an increase in the EGR valve open rate, resulting in a lower peak combustion temperature, and thus has a high correlation with the NOx formation. As shown in Figure 13a, compared with test 1, the engine speed, fuel injection quantity, water temperature, and throttle open rates of test 2 are close, but the air mass quantity is reduced by 60 mg/str, resulting in a 6−10% increase in EGR open rates, which reduces the engine-out NOx emissions from 50 to 20 mg/s. Likewise, Figure 13b shows that the air mass quantity is reduced by 50 mg/str, resulting in a 5−9% increase in EGR open rates, which reduces the engine-out NOx emissions by more than half.

In addition, Figure 14 shows the difference in the EGR valve open rates by the engine operating region between tests 2 and 1 in the rural and motorway phases. Most areas show that the EGR valve open rates of test 2 are higher than those of test 1, especially in the regions of total fuel injection quantity of 20−40 mg/str and engine speed of 1600 to 1800 rpm for both rural and motorway phases, which has a relatively high frequency of engine operation.

3.4. Effect of Postinjection Quantity on NOx Emissions. This section presents the analysis of postinjection quantity on engine-out and tail-pipe NOx emissions. Figure 15 shows the effect of postinjection quantity on the different phases of the RDE tests. The difference in engine-out NOx emissions between test 3 and test 4 is very small, which means the change in postinjection quantity has little influence on engine operating conditions. As for the tail-pipe NOx emissions measured by the PEMS, the total NOx emissions of test 4 are 1.29 times lower than those of test 3, which is attributed to a 2.59 times reduction in the urban phase. Besides, test 4 with increased postinjection quantity can meet the CN6b emission regulations by a significant margin, while test 3 exceeds the standard in the urban phase. This is due to the incomplete combustion reaction of the postinjection quantity injected at the beginning of the expansion stroke after the end of the cylinder compression stroke, which in turn increases the exhaust temperature. Figure 16 shows the comparison of cumulative postinjection quantity and exhaust temperature before the SDPF in the RDE tests between test 3

https://doi.org/10.1021/acsomega.3c03751
ACS Omega 2023, 8, 47452−47462

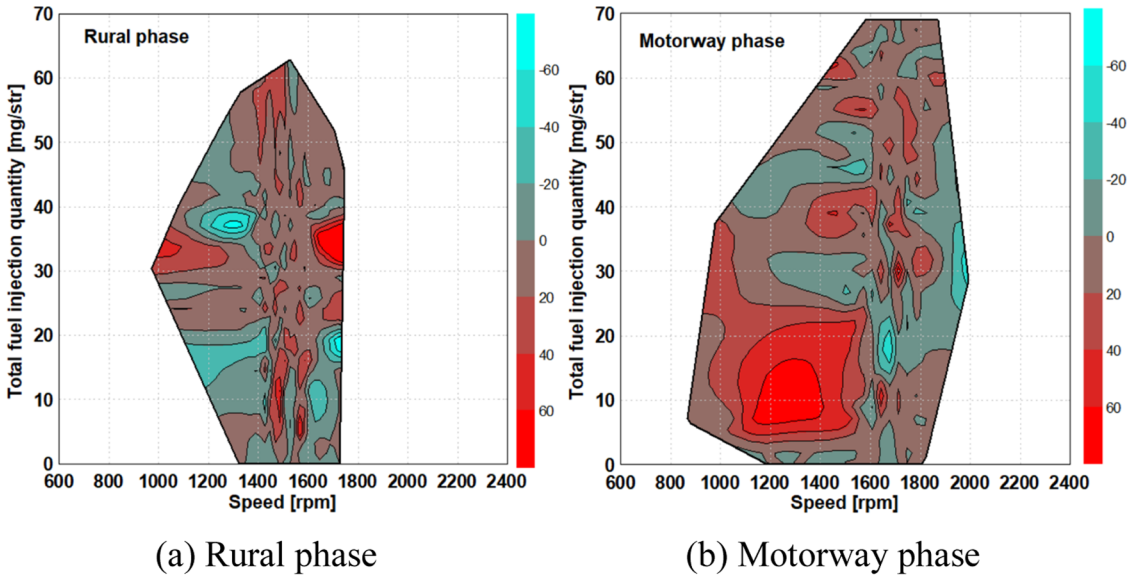

Figure 14. EGR valve open rates difference (test 2−test 1) in rural and motorway phases.

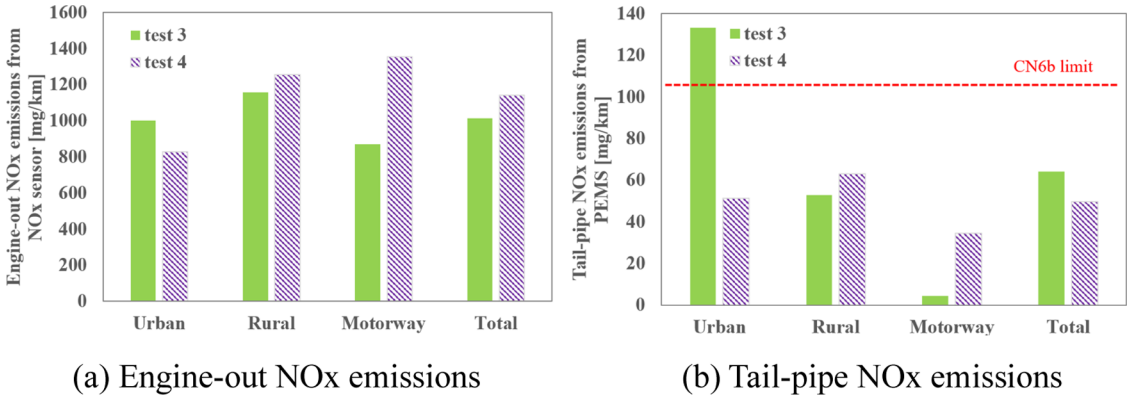

Figure 15. Comparison of engine-out and tail-pipe NOx emissions between test 3 and test 4.

and test 4. As shown in Figure 16, the cumulative postinjection quantity of test 4 increases by 75.4 10.1, and 5.45 g for urban, rural, and motorway phases, respectively, compared to that of test 3. The exhaust temperature before the SDPF of test 4 is generally higher for the urban phase, especially within 600 s after a cold start, and has not much difference for the rural and motorway phases than that of test 3. This is because when the vehicle is driven under the rural and motorway conditions, most of the engine speeds exceed 1600 rpm, which exceeds the operating range of the corrected postinjection quantity mentioned above, rendering the correction function inoperative.

The NOx conversion efficiencies, largely influenced by exhaust temperature,[29] are calculated by the NOx reduction rates upstream and downstream of the catalyst. The NOx conversion efficiencies of tests 3 and 4 are shown in Figure 17. The case of test 4 exhibits a similar overall tendency to the case of test 3 with different phases, with the conversion efficiency over 90% in the rural and motorway phases. Because the urban phase has many stop signs and lower average vehicle speed, its conversion efficiency is lower than the other two phases. The total NOx conversion efficiency between test 4 and test 3 shows a difference of 4.4%, with 7.5, 0.1, and −4.2% for the urban, rural, and motorway phases, respectively. The improvement of NOx conversion efficiency in the urban phase is the main reason for the reduction of tail-pipe NOx emissions.

5. CONCLUSIONS

This paper investigated the potential for reducing engine-out and tail-pipe NOx emissions in the RDE using different control strategies for a light-duty diesel vehicle. NOx sensor values in parts per million or milligrams per km were used for analysis, and PEMS values were used for the evaluation criteria for regulation adoption. The reduction in air mass quantity was introduced to reduce engine-out NOx emissions, and the increase in postinjection was used to minimize tail-pipe NOx emissions. Using both strategies, vehicles can meet the CN6b emission regulations by a significant margin.

The reduction in air mass quantity allowed the engine to operate in larger exhaust gas recirculation (EGR) rate regions, resulting in a 32.5% reduction in engine-out NOx emissions and an 80.4% reduction in tail-pipe NOx emissions. When the engine operated in the regions of adjusted air mass quantity, the EGR valve open rates increased and NOx emissions decreased. This is considered a control strategy to change the combustion state of the engine as the air mass quantity decreases, while the injection quantity remains the same.

https://doi.org/10.1021/acsomega.3c03751
ACS Omega 2023, 8, 47452−47462

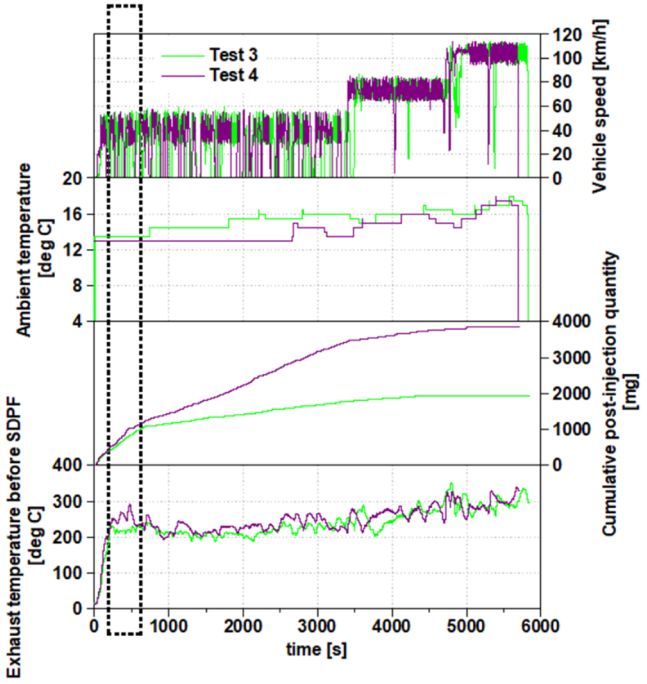

Figure 16. Comparison of cumulative postinjection quantity and exhaust temperature before the SDPF in terms of time between test 3 and test 4; red curve represents test 3 and green curve represents test 4.

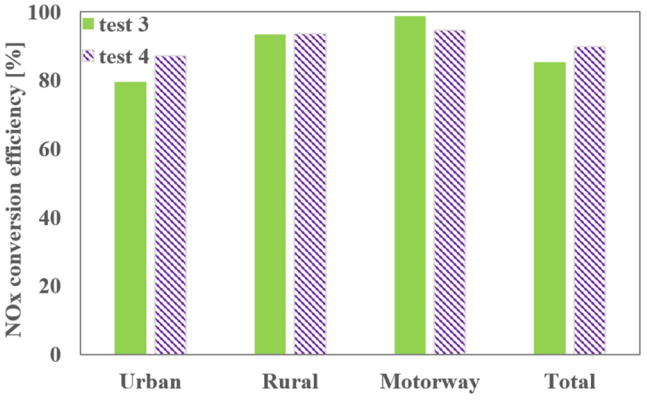

Figure 17. NOx conversion efficiencies of test 3 and test 4.

The increase in postinjection quantity mainly improved the NOx conversion efficiency for the urban phase by 7.5%, leading to a 22.6% reduction in tail-pipe NOx emissions.

Increased postinjection quantity raised the exhaust temperature, especially for the urban phase of an RDE test, which in turn increased the after-treatment conversion efficiency and thus led to excessive NOx emissions.

AUTHOR INFORMATION

Corresponding Author

Yan Su − *State Key Laboratory of Automotive Simulation and Control, Jilin University, Changchun 130025, China; College of Automotive Engineering, Jilin University, Changchun 130025, China;* orcid.org/0000-0001-9126-1692; Email: suyan@jlu.edu.cn

Authors

Jing Chen − *State Key Laboratory of Automotive Simulation and Control, Jilin University, Changchun 130025, China; College of Automotive Engineering, Jilin University, Changchun 130025, China; Jiangxi Isuzu Engine Co., Ltd., Nanchang 330200, China*

Li Xiaoping − *State Key Laboratory of Automotive Simulation and Control, Jilin University, Changchun 130025, China; College of Automotive Engineering, Jilin University, Changchun 130025, China*

Fangxi Xie − *State Key Laboratory of Automotive Simulation and Control, Jilin University, Changchun 130025, China; College of Automotive Engineering, Jilin University, Changchun 130025, China*

Yongzhen Wang − *State Key Laboratory of Automotive Simulation and Control, Jilin University, Changchun 130025, China; College of Automotive Engineering, Jilin University, Changchun 130025, China*

Chuang Yang − *Jiangxi Isuzu Engine Co., Ltd., Nanchang 330200, China*

Complete contact information is available at: https://pubs.acs.org/10.1021/acsomega.3c03751

Notes

The authors declare no competing financial interest.

ACKNOWLEDGMENTS

This work was supported by the National Natural Science Foundation of China (Grant Number U21A20166).

REFERENCES

(1) Kebede, L.; Tulu, G. S.; Lisinge, R. T. Diesel-fueled public transport vehicles and air pollution in Addis Ababa, Ethiopia: effects of vehicle size, age and kilometers travelled. *Atmos. Environ.: X* **2022**, *13*, No. 100144.

(2) Yang, Z.; Liu, Y.; Wu, L.; Martinet, S.; Zhang, Y.; Andre, M.; Mao, H., **2020**. Real-world gaseous emission characteristics of Euro 6b light-duty gasoline- and diesel fueled vehicles. *Transp. Res. : Part D* 78,102215. .

(3) EEA. *European Union Emission Inventory Report 1990−2016 under the UNECE Convention on Long-Range Transboundary Air Pollution (LRTAP)*; European Environment Agency, 2018, DOI: 10.2800/571876.

(4) Kurzydym, D.; Zmudka, Z.; Perrone, D.; Klimanek, A. Experimental and numerical investigation of nitrogen oxides reduction in diesel engine selective catalytic reduction system. *Fuel* **2022**, *313*, No. 122971.

(5) Di Blasio, G.; Ianniello, R.; Beatrice, C.; Pesce, F. C.; Vassallo, A.; Belgiorno, G. Additive manufacturing new piston design and injection strategies for highly efficient and ultra-low emissions combustion in view of 2030 targets. *Fuel* **2023**, *346*, No. 128270.

(6) Yang, M.; Wang, Y. Application of Miller cycle and net-zero fuel(s) to diesel engine: effect on the performance and NOx emissions of a single-cylinder engine. *Energies* **2023**, *16*, 2488.

(7) Kolakoti. Experimental investigation of palm biodiesel on diesel engine combustion performance, cylinder head vibrations and NOx emissions. *J. Mechan. Eng.* **2022**, *19* (1), 273−290.

(8) Di Blasio, G.; Ianniello, R.; Beatrice, C. Hydrotreated vegetable oil as enabler for high-efficient and ultra-low emission vehicles in the view of 2030 targets. *Fuel* **2022**, *310*, No. 122206.

(9) Fayad, M.; Alani, W.; Dhahad, H.; Zheng, J. Diminution of air pollution from NOx and smoke/soot emitted from alcohols/diesel blends in diesel engine and influence of the exhaust gas recirculation (EGR). *J. Environ. Eng. Landscape Manage.* **2022**, *31* (1), 1648−6897.

(10) Fang, Q.; Fang, J.; Zhuang, J.; Huang, Z. Influences of pilot injection and exhaust gas recirculation (EGR) on combustion and emissions in a HCCI-DI combustion engine. *Appl. Therm. Eng.* **2012**, *48*, 97−104.
(11) Nallamothu, R. B.; Nallamothu, A. K.; Nallamothu, S. K.; Injeti, N. K.; Rao, B. Effect of injection timing in multiple injections on NOx and smoke from CRDI diesel engine fueled with biodiesel blend. Ethiopian. *J. Sci. Sustainable Develop.* **2019**, *5* (3), 93−104.
(12) Mohamed, B.; Tewfik, L.; Nasreddine, L. Numerical analysis of injection parameters influence on experimental diesel engine performances and emissions correlated by maximum in-cylinder pressure. *Thermal Sci.* **2023**, *27* (2B), 1479−1493.
(13) Calle-Asensio, A.; Hernandez, J. J.; Fernandez, J. R.; Lapuerta, M.; Ramos, A.; Barba, J. Effect of advanced biofuels on WLTC emissions of a Euro 6 diesel vehicle with SCR under different climatic conditions. *Int. J. Engine Res.* **2021**, *22* (12), 3433−3446.
(14) Kim, H. J.; Jo, S.; Kwon, S.; Lee, J.; Park, S. NOx emission analysis according to after-treatment devices (SCR, LNT + SCR, SDPF), and control strategies in Euro-6 light-duty diesel vehicles. *Fuel* **2022**, *310* (B), No. 122297.
(15) Ko, J.; Jin, D.; Jang, W.; Myung, C.; Kwon, S.; Park, S. Comparative investigation of NOx emission characteristics from a Euro 6-compliant diesel passenger car over the NEDC and WLTC at various ambient temperatures. *Appl. Energy* **2017**, *187* (C), 652−662.
(16) Tutuianu, M.; Bonnel, P.; Ciuffo, B.; Haniu, T.; Ichikawa, N.; Marotta, A.; Pavolvic, J.; Steven, H. Development of the world-wide harmonized light duty test cycle (WLTC) and a possible pathway for its introduction in the European legislation. *Transportation Res., Part D* **2015**, *40* (0), 61−75.
(17) Kurtyka, K.; Pielecha, J.; Merkisz, J. The evaluation of NOx emissions in RDE tests including dynamic driving conditions. *IOP Conf. Ser.: Earth Environ. Sci.* **2021**, *642*, No. 012017.
(18) Chen, Y.; Sun, R.; Kleefeld, J. On-road NOx and smoke emissions of diesel light commercial vehicles − combining remote sensing measurements from across Europe. *Environ. Sci. Technol.* **2020**, *54*, 11744−11752.
(19) Kwon, S.; Park, Y.; Park, J.; Kim, J.; Choi, K.; Cha, J. Characteristics of on-road NOx emissions from Euro 6 light-duty diesel vehicles using a portable emissions measurement system. *Sci. Total Environ.* **2017**, *576*, 70−77.
(20) Wang, Y.; Hao, C.; Ge, Y.; Hao, L.; Tan, J.; Wang, X.; Zhang, P.; Wang, Y.; Tian, W.; Liu, Z.; Li, J. Fuel consumption and emission performance from light-duty conventional/ hybrid-electric vehicles over different cycles and real driving tests. *Fuel* **2020**, *278*, No. 118340.
(21) Yoshida, K.; Kobayashi, H.; Bisaiji, Y.; Oikawa, N.; Fukuma, T. Application and improvement of NOx storage and reduction technology to meet real driving emissions. *Top. Catal.* **2016**, *59*, 845−853.
(22) Prakash, S.; Bodisco, T. An investigation into the effect of road gradient and driving style on NOx emissions from a diesel vehicle driven on urban roads. *Transp. Res.: Part D* **2019**, *72*, 220−231.
(23) Luján, J. M.; Guardiola, P. B.; Pla, B.; Pandey, V. Impact of driving dynamics in RDE test on NOx emissions dispersion. *Proc. Inst. Mech. Eng., Part D* **2020**, *234*, 1770−1778.
(24) Shahariar, G. M.; Sajjad, M.; Suara, K.; Jahirul, M.; Chu-Van, T.; Ristovski, Z.; Brown, R.; Bodisco, T. On-road CO_2 and NOx emissions of a diesel vehicle in urban traffic. *Transp. Res.: Part D* **2022**, *107*, 1361−9209.
(25) Lee, Y.; Lee, S.; Lee, S.; Choi, H.; Min, K. Characteristics of NOx emission of light-duty diesel vehicle with LNT and SCR system by season and RDE phase. *Sci. Total Environ.* **2021**, *782*, No. 146750.
(26) Chen, J.; Su, Y.; Xie, F. Emission Reduction from a light-duty diesel vehicle over two driving cycles through dynamic correction calibration. *ACS Omega* **2023**, *8*, 31772−31783.
(27) Triantafyllopoulos, G.; Katsaounis, D.; Karamitros, D.; Ntziachristos, L.; Samaras, Z. Experimental assessment of the potential to decrease diesel NOx emissions beyond minimum requirements for Euro 6 real drive emissions (RDE) compliance. *Sci. Total Environ.* **2018**, *618*, 1400−1407.
(28) Ministry of Ecology and Environment of the People's Republic of China. Limits and measurement methods for emissions from light-duty vehicles (China 6) 2016 https://www.mee.gov.cn/gkml/hbb/bgg/201612/t20161223_369497.htm (accessed October 21, 2022).
(29) Mohan, S.; Dinesha, P.; Kumar, S. NOx reduction behavior in copper zeolite catalysts for ammonia SCR systems: A review. *Chem. Eng. J.* **2020**, *384*, No. 123253.

https://doi.org/10.1021/acsomega.3c03751
ACS Omega 2023, 8, 47452−47462